NMR reveals hydrogen bonds between oxygen and distal histidines in oxyhemoglobin

Jonathan A. Lukin, Virgil Simplaceanu, Ming Zou, Nancy T. Ho, and Chien Ho*

Department of Biological Sciences, Carnegie Mellon University, Pittsburgh, PA 15213-2683

Edited by Gregory A. Petsko, Brandeis University, Waltham, MA, and approved July 25, 2000 (received for review June 2, 2000)

Compared with free heme, the proteins hemoglobin (Hb) and myoglobin (Mb) exhibit greatly enhanced affinity for oxygen relative to carbon monoxide. This physiologically vital property has been attributed to either steric hindrance of CO or stabilization of O_2 binding by a hydrogen bond with the distal histidine. We report here the first direct evidence of such a hydrogen bond in both α- and β-chains of oxyhemoglobin, as revealed by heteronuclear NMR spectra of chain-selectively labeled samples. Using these spectra, we have assigned the imidazole ring ^{1}H and ^{15}N chemical shifts of the proximal and distal histidines in both carbonmonoxy- and oxy-Hb. Because of their proximity to the heme, these chemical shifts are extremely sensitive to the heme pocket conformation. Comparison of the measured chemical shifts with values predicted from x-ray structures suggests differences between the solution and crystal structures of oxy-Hb. The chemical shift discrepancies could be accounted for by very small displacements of the proximal and distal histidines. This suggests that NMR could be used to obtain very high-resolution heme pocket structures of Hb, Mb, and other heme proteins.

Human normal adult Hb (Hb A) is one of the most thoroughly studied proteins and serves as a paradigm for multimeric, allosteric proteins. During the past several decades, extensive research has been devoted to correlating the conformation of Hb A with its functional properties, especially the cooperative binding of oxygen and the control of oxygen affinity by pH (the Bohr effect), as well as allosteric effectors, such as 2,3-bisphosphoglycerate. Despite these efforts, the precise molecular basis for the cooperative oxygenation process of Hb A remains controversial (1–5). According to the crystal structure of the Hb molecule, two regions are particularly important for the allosteric control of ligand binding: the heme pockets, where ligation initiates structural changes, and the $\alpha_1\beta_2$ interface, where the largest conformational changes occur. In this article, we focus on the conformation of the heme pockets, as revealed by NMR spectroscopy.

Much of our present understanding of the structure–function relationship of Hb A is based on the x-ray crystal structures of unliganded (6) and liganded (7, 8) Hb. The classical mechanism proposed by Perutz (9) for cooperative oxygen binding identifies these structures with the T (low-affinity) and R (high-affinity) states in the two-state Monod–Wyman–Changeux model (10) and implicitly assumes that they represent the structures of deoxy- and oxy-Hb inside red blood cells under physiological conditions.

The observation of a third quaternary structure of Hb A has cast doubt on the two-structure concerted model for the oxygenation of Hb A. This new conformation, R2, has been seen in carbonmonoxy-Hb A (HbCO A) in low salt conditions at pH 5.8 (11), as well as in cyanomet-Hb A crystallized under physiological salt and pH conditions (0.1 M Tris/0.1 M NaCl/1 mM Na_2EDTA/1 mM KCN, pH 7.4, with 0.12% β-octyl glucoside and 16–17% polyethylene glycol 8000) (12). Geometric analysis (13) suggests that the R structure may be an intermediate form, which lies on the path between T and R2. As indicated by its functional properties, the quaternary structure of Hb A in solution is the result of a delicate balance involving anion concentration, pH, and other buffer conditions. There is evidence that HbCO A in solution undergoes conformational exchange among an ensemble of structures (G. Kontaxis and A. Bax, personal communication). Crystallization under particular conditions may select for a specific structure, which may not be among the most accessible conformations in solution (14). Therefore, to correlate the function of Hb A with its structure at atomic resolution, it is necessary to determine the solution structure and dynamic properties of Hb A under physiological conditions.

Proteins as large as Hb A (64.5 kDa) are now being brought within the scope of multidimensional, multinuclear NMR spectroscopy. This technique requires labeling of samples with ^{2}H, ^{15}N, and/or ^{13}C, which is performed using an *Escherichia coli* expression system for Hb A (15, 16). We have recently reported the use of a chain-selective labeling technique to obtain better-resolved, less ambiguous NMR spectra (17). Chain-selectively ^{15}N-labeled samples have been used to assign the imidazole side-chain ^{1}H and ^{15}N resonances of all 38 histidines (19 per $\alpha\beta$ dimer), as well as the $H\delta_1$, $H\varepsilon_1$, and $N\varepsilon_1$ resonances of all six tryptophans of HbCO A (17). We report here the results of similar experiments on HbO_2 A and compare observed NMR chemical shifts with values predicted from published x-ray structures of Hb A.

Materials and Methods

Sample Preparation. Uniformly ^{15}N-labeled recombinant Hb A was obtained by expression from the plasmid pHE2, and the α- and β-chains were separated as previously described (15–17). Chain-selectively ^{15}N-labeled Hb A was prepared by mixing equal molar quantities of either ^{15}N-labeled α-chain or β-chain with the complementary unlabeled chain. The chain-selectively labeled Hb A was then equilibrated with the appropriate buffer for NMR studies. The HbCO A samples were at pH 6.5 in 0.05 M sodium phosphate, and the HbO_2 A samples were at pH 8.0 in 0.1 M sodium phosphate. Such a basic buffer was necessary to inhibit oxidation of the HbO_2 A samples during the 10–18 h required for each 2D-NMR experiment.

NMR Experiments. Echo anti-echo (^{1}H, ^{15}N) heteronuclear multiple quantum coherence (HMQC) experiments were performed on a Bruker Avance DRX-600 spectrometer as previously described (17). All experiments were performed at 29°C. Several HMQC spectra were acquired with a ^{15}N carrier frequency of

This paper was submitted directly (Track II) to the PNAS office.

Abbreviations: Hb A, human normal adult Hb; HbCO A, carbonmonoxy-Hb A; PDB, Protein Data Base; MbCO, carbonmonoxymyoglobin; HMQC, heteronuclear multiple quantum coherence; Mb, myoglobin.

*To whom reprint requests should be addressed at: Department of Biological Sciences, Carnegie Mellon University, 4400 Fifth Avenue, Pittsburgh, PA 15213-2683. E-mail: chienho@andrew.cmu.edu.

The publication costs of this article were defrayed in part by page charge payment. This article must therefore be hereby marked "*advertisement*" in accordance with 18 U.S.C. §1734 solely to indicate this fact.

Article published online before print: *Proc. Natl. Acad. Sci. USA*, 10.1073/pnas.190254697. Article and publication date are at www.pnas.org/cgi/doi/10.1073/pnas.190254697

160 ppm, a spectral width in ^{15}N of 200 ppm, and a refocusing delay of 5.2 ms, to observe directly bonded ^{1}H–^{15}N cross-peaks. An additional HMQC spectrum of ^{15}N-α-labeled HbO_2 A was obtained with a refocusing delay of 10.4 ms, which diminished the intensity of the directly bonded ^{1}H–^{15}N cross-peaks (including those of the backbone amides) while retaining the cross-peaks due to two- and three-bond correlations. This spectrum was acquired with a ^{15}N carrier frequency of 205 ppm and a spectral width of 110 ppm, which caused the residual backbone amide peaks to appear folded, with ^{15}N chemical shifts between 220 and 240 ppm. Finally, to emphasize the weak $H\varepsilon_1$ and $H\delta_2$ peaks of the distal histidines that are normally obscured by the ($H\varepsilon_2$,$N\varepsilon_2$) cross-peaks, an HMQC experiment was performed on fully ^{15}N-labeled HbO_2 A dissolved in >98% D_2O, using a ^{15}N carrier frequency of 200 ppm, a spectral width in ^{15}N of 120 ppm, and a refocusing delay of 5.2 ms.

Chemical Shift Prediction: A Test of the Method. Predicted ^{1}H chemical shifts were calculated from x-ray crystal structures of Hb [in the form of Protein Data Base (PDB) files], using the program TOTAL.F (provided by Dr. Michael P. Williamson of the Department of Molecular Biology and Biotechnology, University of Sheffield, Sheffield, UK, on his web page at http://www.shef.ac.uk/uni/projects/nmr/resources.html). This program takes into account magnetic anisotropy, electric field effects, and ring-current shifts, adding these to the random-coil proton shifts to predict the net ^{1}H chemical shifts. To check the accuracy of this program, we have applied it to a recent high-resolution crystal structure of carbonmonoxymyoglobin (MbCO) [PDB entry 1BZR (18)] and tabulated the difference between predicted chemical shifts and those assigned by Theriault *et al.* (19). Excluding the backbone amides, the standard deviation of the chemical shift error was $\sigma = 0.32$ ppm. Ninety percent of the predicted chemical shifts are within 0.5 ppm of the assigned shifts. The maximum error for the imidazole ^{1}H chemical shifts of the proximal and distal histidyl residues of MbCO was 0.46 ppm. The results of this test indicate that Williamson's program can accurately predict the chemical shifts of protons, particularly those of histidyl protons near the heme.

Results and Discussion

HMQC Spectra Reveal Tautomeric States of Histidyl Residues. Parts of the echo anti-echo HMQC spectra of chain-selectively ^{15}N-labeled oxy- and carbonmonoxy-Hb A are shown superimposed in Fig. 1. The protonated ^{15}N of a histidyl imidazole ring has a chemical shift of roughly 160 ppm, whereas the bare ^{15}N resonates further downfield, around 250 ppm (20). In general, both nitrogens in the ring are coupled to both carbon-bound protons, resulting in a rectangular pattern of four cross-peaks in the HMQC spectrum; the three of these that correspond to two-bond couplings will be relatively intense. A less intense or missing cross-peak is diagnostic of the weak three-bond ($H\delta_2$, $N\delta_1$) coupling. For distal α58His in HbCO A, the missing cross-peak at the lower right-hand corner of the rectangle [at (4.51, 250.6) ppm] thus indicates that these chemical shifts can be assigned to ($H\delta_2$, $N\delta_1$). The chemical shift of $N\delta_1$ shows that it is unprotonated, i.e., this histidyl residue exists in the ε tautomeric state, as illustrated in the inset to Fig. 1. The same argument applies for distal β63His. For the proximal histidines α87His and β92His, however, the weak or missing cross-peak is in the upper right-hand corner of the rectangle, consistent with $N\delta_1$ being protonated, whereas $N\varepsilon_2$ is bonded to the heme Fe, as shown in Fig. 2. Our finding of a protonated $N\varepsilon_2$ for both distal histidines of HbO_2 is in contrast to the observation of the alternative (δ) tautomer in a neutron crystal structure of MbCO (21). However, Phillips and co-workers (22) have suggested that the protonated $N\delta_1$ seen in the neutron structure is actually due to the aquomet form, resulting from oxidation of the MbCO crystal sample. These researchers have presented strong evidence in favor of the $N\varepsilon_2$–H tautomer, on the basis of correlations between the calculated electrostatic fields and observed FeCO stretching frequencies of mutant and wild-type myoglobins (22).

Heme-Pocket Conformational Differences in HbCO A and HbO_2 A. Strong, broad doublet cross-peaks appear for protons directly bound to nitrogens of those histidines for which the exchange rate with solvent (water) protons is much slower than the one-bond scalar coupling, J. Most of the sharp cross-peaks with ^{1}H chemical shifts between 6.3 ppm and 8.6 ppm originate from multiple-bond couplings within the solvent-exposed histidines of Hb A (17). There are no corresponding NH doublet cross-peaks for these histidines because of fast (submillisecond) exchange with the water protons, which makes these histidyl residues sensitive to the pH of the solution. Here, we focus on the proximal (α87His and β92His) and distal (α58His and β63His) histidines. The cross-peaks of these residues can be identified as such by their disappearance in the spectrum of deoxy-Hb A (results not shown), because of their proximity to the paramagnetic heme iron. The peaks corresponding to the proximal histidines in the spectra of HbO_2 A show marked differences in both ^{1}H and ^{15}N chemical shifts as compared with those of HbCO A, but only minor differences between the α- and β-heme pockets. Among the features apparent in Fig. 1 is the near-degeneracy of resonances from the α- and β-subunits in HbCO A, indicating that the histidines in the α- and β-heme pockets experience nearly identical environments. In contrast, the cross-peaks of the distal α- and β-histidines in the spectra of HbO_2 A exhibit a wide separation in the ^{1}H dimension. Thus, conformational differences between the α- and β-distal heme pockets are more marked in HbO_2 A than in HbCO A. These conformational differences may account for the difference in the binding of CO and O_2 to Hb A. Johnson and Ho (23) reported that CO exhibits random binding between the α- and β-hemes of Hb A in the absence and presence of 2,3-bisphosphoglycerate, whereas O_2 exhibits a preferential binding to the α-hemes, especially in the presence of 2,3-bisphosphoglycerate.

Evidence for Distal His–O_2 H-bonds in Oxy-Hb. The pattern of cross-peaks for the distal histidines in the HMQC spectrum of HbCO A indicates that $N\varepsilon_2$ is protonated (17, 20), but no doublet cross-peak characteristic of an NH moiety can be detected, presumably because of exchange with a water molecule in the distal heme pocket. However, such doublets are clearly visible in the spectrum of HbO_2 A, at ^{1}H chemical shifts of 4.8 ppm and 5.4 ppm (Fig. 1). This indicates that the $H\varepsilon_2$ proton is stabilized against solvent exchange by a H-bond between the distal His and the O_2 ligand in both the α- and β-subunits. An analogous H-bond has been observed in MbO_2 by neutron diffraction (24). Its existence in Hb has been suggested by ^{1}H- and ^{17}O-NMR spectroscopy of small model compounds (25, 26) as well as electron spin resonance and resonance Raman spectroscopy of cobalt-substituted HbO_2 (27, 28). To our knowledge, however, the HMQC spectra shown in Fig. 1 provide the first direct evidence of a distal histidyl H-bond in HbO_2 A. Such an H-bond has been implicated in stabilizing the binding of O_2 to Hb and Mb, relative to free heme (29), and has been the subject of some controversy (30).

Proposed Mechanisms of Ligand Discrimination in Heme Proteins. An important function of both Hb and Mb is to modulate the affinity of the heme for ligands such as O_2, CO, and NO. The relative affinity of CO and O_2 is expressed in terms of the ratio of equilibrium binding constants $M \equiv K_{CO}/K_{O2}$, which is roughly 2×10^4 for unencumbered model heme compounds in organic solvents (31). Such a strong preference for CO binding would

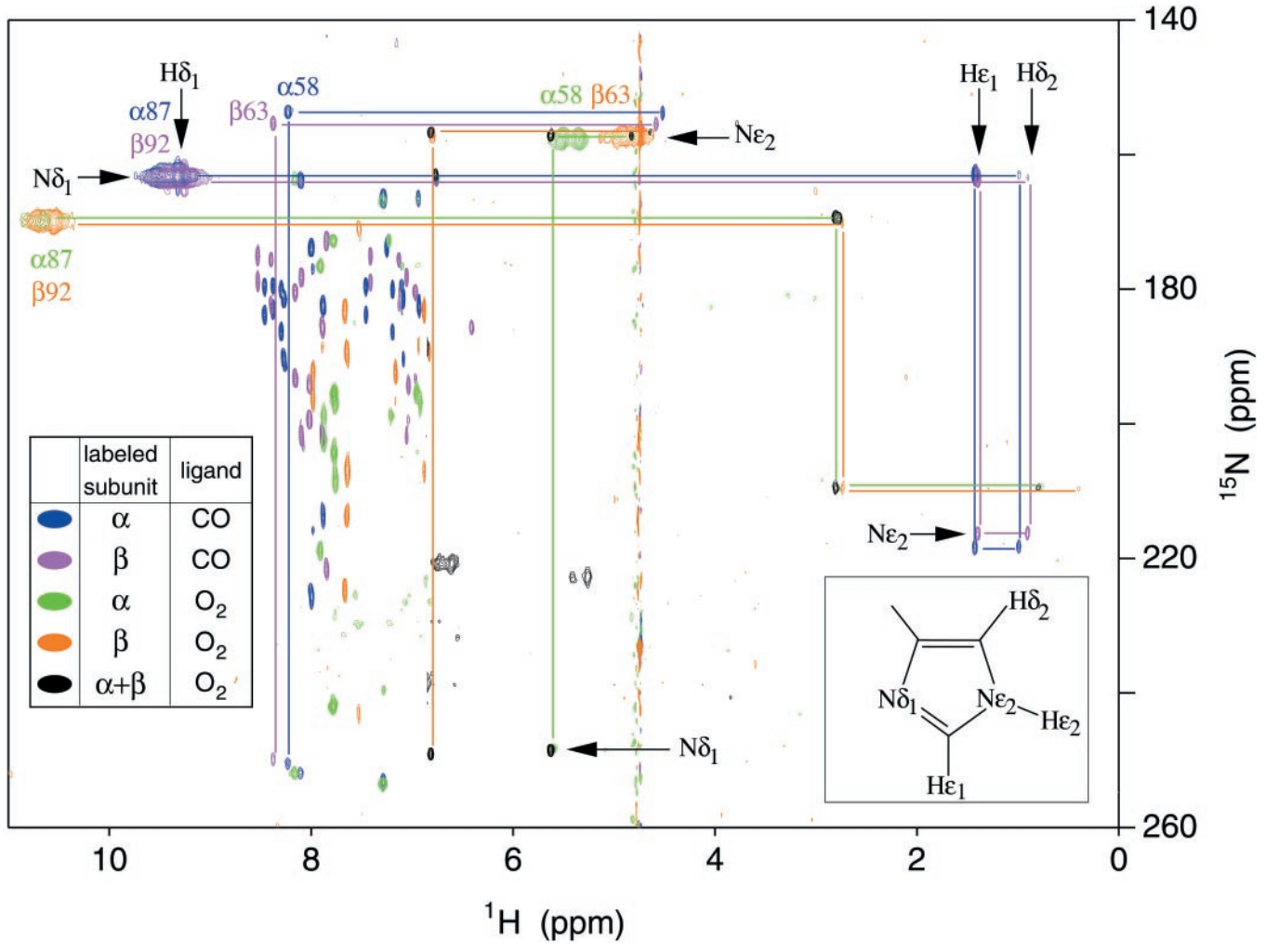

Fig. 1. Histidine region of the 600-MHz (^{1}H, ^{15}N) echo anti-echo HMQC spectra of chain-selectively and fully ^{15}N-labeled HbCO A and HbO_2 A in water and D_2O at 29°C. Cross-peaks in blue, violet, green, and orange come from spectra of (15)N-α-labeled HbCO A, (15)N-β-labeled HbCO A, (15)N-α-labeled HbO_2 A, and (15)N-β-labeled HbO_2 A, respectively. These experiments used a large spectral width in ^{15}N and a short refocusing delay (see *Materials and Methods* for details). The spectra were acquired without ^{15}N decoupling; therefore doublets are observed for directly bonded (15)N-^{1}H pairs. Also shown in green is a spectrum of (15)N-α-labeled HbO_2 A with a smaller ^{15}N spectral width and a longer refocusing delay, set to eliminate the α58His ($H\varepsilon_2$, $N\varepsilon_2$) doublet, which overlaps the $H\varepsilon_1$ cross-peak at 5.64 ppm. Cross-peaks in black are those of fully ^{15}N-labeled HbO_2 A in D_2O solution, which used a narrow ^{15}N spectral width and a short refocusing delay. Cross-peaks originating from the same residue are connected by lines. Other cross-peaks originate from the solvent-exposed and interfacial histidyl residues not discussed in this paper (see ref. 17 for details).

inhibit the oxygen storage and transport functions of Mb and Hb in the presence of low levels of CO, which is produced endogenously by the catabolic breakdown of heme proteins (32). Fortunately, the binding affinity of O_2 relative to that of CO is strongly enhanced in Hb A and Mb, which reduce the value of M to approximately 250 and 25, respectively (29). This physiologically vital effect was originally attributed (32) to destabilization of bound CO due to steric hindrance, on the basis of early x-ray crystal structures, which showed an unfavorable, bent orientation for CO bound to both Mb and Hb. This mechanism was disputed by Spiro and co-workers (33, 34), who pointed out that a large degree of Fe–CO bending was inconsistent with observed vibrational spectra and would require stronger steric forces than a polypeptide is capable of exerting. More recent x-ray structures of Mb (18, 35) suggest a modest off-axis distortion of the ligand, which can be realized at a lower energetic cost if tilting of the Fe–C bond and buckling of the heme occur together with Fe–C–O bending (33).

An upright, perpendicular geometry of the CO group is indicated by time-resolved IR polarization spectroscopy (36) of MbCO, as well as a joint analysis of NMR, ^{57}Fe Mössbauer, and IR data, using density functional theory (37). Any remaining discrepancy between this model and recent x-ray structures is reconciled by density functional theory calculations (38), which show that the transition dipole of the C–O stretching IR band is not coincident with the C–O bond vector, but lies between the Fe–C bond vector and the heme perpendicular. The minimum energy structure consistent with the measured IR transition dipole is slightly tilted and bent, giving an off-axis displacement of the oxygen atom that is within the distribution seen in MbCO crystal structures. Steric distortion may still play a part in lowering the CO affinity of Mb, as the binding of the ligand in a nearly upright orientation may require displacement of distal residues (39) or concerted motion of protein helices (18). On the basis of density functional theory calculations (38) and studies of mutant myoglobins (29, 40), steric hindrance by the distal histidine accounts for ≈1.0 kcal/mol, or roughly 25% of myoglobin's discrimination against CO relative to O_2.

Rather than steric constraints hindering the binding of CO, an alternative explanation for the reduced value of M in heme

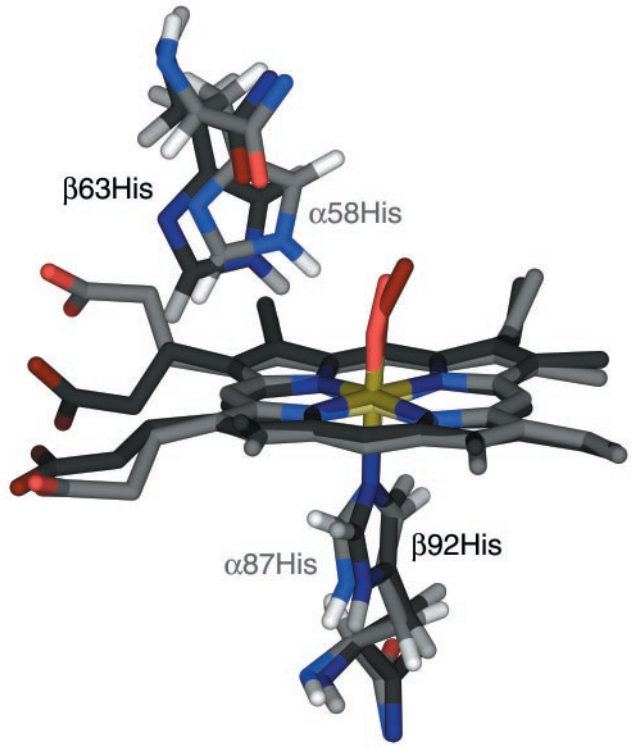

Fig. 2. Proximal and distal histidyls of the HbO_2 A x-ray crystal structure (PDB entry 1HHO; ref. 8), with the hemes of the α- and β-subunits superimposed. The coordinates of hydrogen atoms were calculated from those of heavy atoms, using standard bond lengths and angles. The α- and β-subunits are shown in lighter and darker colors, respectively. This structure suggests that the distal histidine in the α-subunit is better disposed to form a H-bond with the O_2 ligand than is its counterpart in the β-subunit.

proteins is that electrostatic interactions and hydrogen-bonding favor the binding of O_2. In the complex of O_2 with ferrous heme, the bound ligand is highly polar, with characteristics of the superoxide anion (31), allowing it to form a strong H-bond with the distal histidine. In deoxy-Mb, a water molecule hydrogen-bonded to the distal histidine must be displaced for either CO or O_2 to bind (18, 40, 41). Whereas O_2 forms a much stronger H-bond with the distal histidine, CO forms (at most) a very weak one. Thus, the presence of the distal histidine causes a ~100-fold increase in O_2 affinity together with a ~10-fold decrease in CO affinity, which account for the 1000-fold reduction of M for mammalian myoglobins relative to simple chelated protohemes (29). Our observation of distal histidine–ligand H-bonds in HbO_2 A, but not in HbCO A supports a similar mechanism for the less dramatic ligand selectivity of Hb.

Comparison of Observed and Calculated Chemical Shifts. The chemical shifts of the proximal and distal histidines are extremely sensitive to their orientation with respect to the nearby heme, because of strong ring-current effects created by the porphyrin. Thus, these amino acid residues can serve as probes of the heme-pocket conformation. The HMQC spectra can be correlated with the structure of Hb with the aid of a computer program, TOTAL.F, which, given a protein's structure in the form of a PDB file, predicts the ^1H chemical shifts (42, 43). The predicted chemical shifts of the proximal and distal histidines are compared with our experimental results in Table 1. Chemical shifts were calculated by applying the program described above to several x-ray crystal structures of liganded Hb: the structure of HbCO A in the R state (7) [PDB entry 2HCO], the structure

Table 1. Calculated and observed chemical shifts (ppm) for distal and proximal histidines of HbCO A and HbO_2 A

	HbCO A			HbO_2 A	
Chem. shift assignment	2HCO, ppm	1BBB, ppm	obs., ppm	1HHO, ppm	obs., ppm
α58His Hδ_2	4.90	4.83	4.51	4.89	4.83
β63His Hδ_2	5.16	4.91	4.58	4.93	4.65
α58His Hε_1	8.48	8.34	8.23	7.15	5.64
β63His Hε_1	8.14	8.50	8.38	8.12	6.81
α58His Hε_2	7.42	5.65	*	5.36	5.42
β63His Hε_2	5.63	5.62	*	5.26	4.79
α87His Hδ_1	10.04	9.46	9.42	9.78	10.73
β92His Hδ_1	9.13	9.47	9.34	8.65	10.64
α87His Hδ_2	1.25	1.66	1.00	1.42	0.77
β92His Hδ_2	1.27	1.70	0.90	0.88	0.40
α87His Hε_1	1.87	1.41	1.43	1.70	2.77
β92His Hε_1	1.54	1.85	1.39	1.86	2.74
rms deviation	0.38	0.39	—	0.99	—

Chemical shifts of corresponding protons in the α- and β-subunits are listed in adjacent rows. The last row lists the rms deviation between the observed chemical shifts and those calculated for each structure.
*Not observed in HbCO A, because of rapid exchange of the distal histidine Hϵ_2 with water.

of HbCO A in the R2 conformation (11) [1BBB], and the R-state structure (8) of HbO_2 A [1HHO]. The observed chemical shifts of HbCO A are in good overall agreement with those calculated from both the R and R2 conformations, with rms deviations of 0.38 ppm and 0.39 ppm, respectively.

It is also interesting to examine the differences between corresponding chemical shifts in the α- and β-subunits (e.g., β92His Hδ_1–α87His Hδ_1). From observations of HbCO A, we can tabulate α–β chemical shift differences for five types of protons: Hδ_2 and Hε_1 for the distal histidines, and Hδ_1, Hδ_2, and Hε_1 for the proximal histidines. When these values are compared with chemical shift differences calculated from x-ray structures, the resulting rms deviations are 0.46 ppm and 0.23 ppm for the R and R2 conformations, respectively. Note that this type of comparison eliminates any uncertainty in the value of the "random coil" shift of each type of proton. Thus, the differences between the α- and β-heme pocket conformations seem to be more accurately represented by the R2 structure than the R structure.

Heme-Pocket Conformational Differences Between Solution and Crystalline States of HbO_2 A. In the spectrum of HbO_2 A, the Hε_1 resonances of the distal histidines are separated by about 1.1 ppm, indicating a greater difference between the distal α- and β-heme pockets in oxy- than in carbonmonoxy-Hb A, where these resonances are nearly degenerate. A similar separation (of 1.2 ppm) is predicted from the x-ray structure (8) (1HHO), but the calculated chemical shifts are approximately 1.4 ppm higher than the observed values. The predicted chemical shifts of the proximal and distal histidyl residues of HbO_2 A are in relatively poor agreement with the observed chemical shifts. Whereas our NMR spectra show H-bonds between O_2 and the distal histidine in both subunits, the x-ray structure, as illustrated in Fig. 2, suggests such a H-bond in the α-subunit, but "either none or a weak one in the β-subunit" (8). When hydrogen atoms are added to the x-ray structure of HbO_2 A, α58His Hε_2 is 1.72 Å away from the terminal oxygen of the O_2 ligand, and the atoms Nε_2–Hε_2–O form an angle of 139°. The corresponding distance and angle for β63 His are 2.86 Å and 120°, indicating a less favorable geometry for a hydrogen bond in the β-subunit.

These results suggest that the solution conformation of the

heme pockets differs from the 2.1-Å x-ray structure of HbO_2 A, which was determined using crystals grown at high salt concentrations (2.5 M phosphate, pH 6.7). An important lesson to be learned from the history of the "bent CO" in Hb and Mb is that x-ray structures refined to moderate resolution should not be taken as exact. As noted above, chemical shifts of amino acid residues near the heme are very sensitive to heme-pocket conformation. For example, if α58His in the x-ray structure of HbO_2 A is displaced by only 0.2 Å across the face of the heme, its $H\varepsilon_1$ and $H\varepsilon_2$ chemical shifts are predicted to change by -0.47 ppm and -0.23 ppm, respectively; changes that are easily detectable in NMR spectra. Thus, NMR is capable of revealing extremely precise structural information for the heme pocket under physiological conditions and may help elucidate the mechanisms for allosteric control and discrimination among ligands essential to Hb function.

We thank Dr. Michael P. Williamson for making his computer program TOTAL.F available, Dr. Ming F. Tam for carrying out our N-terminal analyses by Edman degradation and electrospray ionization mass spectrometric analyses to evaluate our recombinant hemoglobin samples, Dr. Ad Bax for providing information before publication, and Dr. William R. McClure and Dr. Gordon S. Rule for helpful discussions. This work was supported by U.S. Public Health Service grants (R01HL245215 and S10RR11248).

1. Ackers, G. K. (1998) *Adv. Protein Chem.* **51,** 185–253.
2. Shibayama, N., Moromoto, H. & Saigo, S. (1998) *Biochemistry* **37,** 6221–6228.
3. Perutz, M. F., Wilkinson, A. J., Paoli, M. & Dodson, G. G. (1998) *Annu. Rev. Biophys. Biomol. Struct.* **27,** 1–34.
4. Eaton, W. A., Henry, E. R., Hoffrichter, J. & Mozzarelli, A. (1999) *Nat. Struct. Biol.* **6,** 351–358.
5. Ho, C. & Lukin, J. A. (2000) in *Embryonic Encyclopedia of Life Sciences* (Macmillan Reference, London).
6. Fermi, G., Perutz, M. F., Shaanan, B. & Fourme, R. (1984) *J. Mol. Biol.* **175,** 159–194.
7. Baldwin, J. M. (1980) *J. Mol. Biol.* **136,** 103–128.
8. Shaanan, B. (1983) *J. Mol. Biol.* **171,** 31–59.
9. Perutz, M. F. (1970) *Nature (London)* **228,** 726–739.
10. Monod, J., Wyman, J. & Changeux, J. P. (1965) *J. Mol. Biol.* **12,** 88–118.
11. Silva, M. M., Rogers, P. H. & Arnone, A. (1992) *J. Biol. Chem.* **267,** 17248–17256.
12. Smith, F. R. & Simmons, K. C. (1994) *Proteins* **18,** 295–300.
13. Srinivasan, R. & Rose, G. D. (1994) *Proc. Natl. Acad. Sci. USA* **90,** 11113–11117.
14. Tame, J. R. H. (1999) *Trends Biochem. Sci.* **24,** 372–377.
15. Shen, T.-J., Ho, N. T., Simplaceanu, V., Zou, M., Green, B. N., Tam, M. F. & Ho, C. (1993) *Proc. Natl. Acad. Sci. USA* **90,** 8108–8112.
16. Shen, T. J., Ho, N. T., Zou, M., Sun, D. P., Cottam, P. F., Simplaceanu, V., Tam, M. F., Bell, D. A., Jr. & Ho, C. (1997) *Protein Eng.* **10,** 1085–1097.
17. Simplaceanu, V., Lukin, J. A., Fang, T.-Y., Zou, M., Ho, N. T. & Ho, C. (2000) *Biophys. J.* **79,** 1146–1154.
18. Kachalova, G. S., Popov, A. N. & Bartunik, H. D. (1999) *Science* **284,** 473–476.
19. Theriault, Y., Pochapsky, T. C., Dalvit, C., Chiu, M. L., Sligar, S. G. & Wright, P. E. (1994) *J. Biomol. NMR* **4,** 491–504.
20. Pelton, J. G., Torchia, D. A., Meadow, N. D. & Roseman, S. (1993) *Protein Sci.* **2,** 543–558.
21. Cheng, X. D. & Schoenborn, B. P. (1991) *J. Mol. Biol.* **220,** 381–399.
22. Phillips, G. N., Jr., Teodoro, M. L., Li, T., Smith, B. & Olson, J. S. (1999) *J. Phys. Chem. B* **103,** 8817–8829.
23. Johnson, M. E. & Ho, C. (1974) *Biochemistry* **13,** 3653–3661.
24. Phillips, S. E. V. & Schoenborn, B. P. (1981) *Nature (London)* **292,** 81–82.
25. Mispelter, J., Momenteau, M., Lavalette, D. & Lhoste, J.-M. (1983) *J. Am. Chem. Soc.* **105,** 5165–5166.
26. Gerothanassis, I. P., Momenteau, M. & Loock, B. (1989) *J. Am. Chem. Soc.* **111,** 7006–7012.
27. Yonetani, T., Yamamoto, H. & Iizuka, T. (1974) *J. Biol. Chem.* **249,** 2168–2174.
28. Kitagawa, T., Ondrias, M. R., Rousseau, D. L., Ikeda-Saito, M. & Yonetani, T. (1982) *Nature (London)* **298,** 869–871.
29. Springer, B. A., Sligar, S. G., Olson, J. S. & Phillips, G. N., Jr. (1994) *Chem. Rev.* **94,** 699–714.
30. Borman, S. (1999) *Chem. Eng. News* **77,** 31–35.
31. Olson, J. S. & Phillips, G. N., Jr. (1997) *J. Biol. Inorg. Chem.* **2,** 544–552.
32. Collman, J. P., Brauman, J. I., Halbert, T. R. & Suslick, K. S. (1976) *Proc. Natl. Acad. Sci. USA* **73,** 3333–3337.
33. Li, X.-Y. & Spiro, T. G. (1988) *J. Am. Chem. Soc.* **110,** 6024–6033.
34. Ray, G. B., Li, X.-Y., Ibers, J. A., Sessler, J. L. & Spiro, T. G. (1994) *J. Am. Chem. Soc.* **116,** 162–176.
35. Vojtechovsky, J., Chu, K., Berendzen, J., Sweet, R. M. & Schlichting, I. (1999) *Biophys. J.* **77,** 2153–2174.
36. Lim, M., Jackson, T. A. & Anfinrud, P. A. (1995) *Science* **269,** 962–966.
37. McMahon, M. T., deDios, A. C., Godbout, N., Salzmann, R., Laws, D. D., Le, H. B., Havlin, R. H. & Oldfield, E. (1998) *J. Am. Chem. Soc.* **120,** 4784–4797.
38. Spiro, T. G. & Kozlowski, P. M. (1998) *J. Am. Chem. Soc.* **120,** 4524–4525.
39. Sage, J. T. (1997) *J. Biol. Inorg. Chem.* **2,** 537–543.
40. Quillin, M. L., Arduini, R. M., Olson, J. S. & Phillips, G. N., Jr. (1993) *J. Mol. Biol.* **234,** 140–155.
41. Quillin, M. L., Li, T., Olson, J. S., Phillips, G. N., Jr., Dou, Y., Ikeda-Saito, M., Regan, R., Carlson, M., Gibson, Q. H., Li, H., *et al.* (1995) *J. Mol. Biol.* **245,** 416–436.
42. Williamson, M. P. & Asakura, T. (1993) *J. Magn. Reson.* **B 101,** 63–71.
43. Asakura, T., Taoka, K., Demura, M. & Williamson, M. P. (1995) *J. Biomol. NMR* **6,** 227–236.